Article in Press: JJEES 16(2), June 2025.
This article has been accepted for publication and will appear in the upcoming issue. The final published version will be available through the journal website after copyediting, typesetting and proofreading.

Integrating Optical and SAR Sentinel Data for Improved Land Cover Mapping in Northeastern Region of Pakistan

Iftikhar Ahmad Khan[1*] and Junaid Aziz Khan[2]

1. Forest Department, Muzaffarabad-AJK, Pakistan
2. National University of Science & Technology (NUST)Islamabad, Pakistan, email: Junaid@igis.nust.edu.pk

Received on January 19, 2023, Accepted on January 12, 2025

Abstract

Accurate Land Use Land Cover (LULC) mapping is important for the planning and management of natural and manmade resources. Though widely used remote sensing data has largely facilitated land cover mapping from global to local scale, generally used optical data has some inherent limitations which can be compensated to some extent through the use of synergistically combined optical and SAR data. Ever-evolving data fusion techniques have encouraged the combined use of SAR and optical data for LULC classification. In this study, three different classification scenarios were analyzed. In the first and second cases, Sentinel-1 (S1) and Sentinel-2 (S2) data alone were tested, then, as a third step, integrated Optical-SAR dataset (S1+S2) with varying combinations of S1 & S2 input variables was evaluated for LULC mapping. In the case of Sentinel-1 SAR data, our results produced an overall accuracy (OA), ranging from 44.6% -63.01% with Kappa Coefficient (KC) of 0.33-0.55 where SAR-based Grey Level Co-occurrence Matrix (GLCM) textures contributed significantly toward increasing classification accuracy. In the spectral domain, the accuracy range spanned from 86% (KC=0.83) to 89.59% (KC=0.87), whereas a combined dataset that included features from both SAR and Optical sides yielded the highest overall accuracy of 93.12% with KC= 0.91.

Keywords: Sentinel-1, Sentinel-2, GLCM Textures, Data Fusion, Random Forest, Land Cover Mapping

* Corresponding author e-mail address: ik188960@gmail.com

Article in Press: JJEES 16(2), June 2025.
This article has been accepted for publication and will appear in the upcoming issue. The final published version will be available through the journal website after copyediting, typesetting and proofreading. ©2025 JJEES.

1. INTRODUCTION

The concepts of land use and land cover (LULC) have been elaborately explained in the literature. Water, soil, and vegetation that constitute the biophysical cover of Earth's surface are identified as land cover, whereas land cover is exploited by humans for the purpose of land use (Lambin et al., 2000). Land cover maps serve as a source of practical information for multiple usages (Abdikan et al., 2016), and LULC detection and mapping is considered essential for many socio-economic and environmental applications that include conservation and management of natural resources, agricultural and forest monitoring, urban planning, estimation of crop yield, detection of oil spills, and mapping of catastrophic events like wildfires, tsunamis, and floods (Kavitha et al., 2021).

Utilizing Remote Sensing with its different forms has many advantages, such as (1) extensive pre-existing databases like Landsat, Sentinel-1, sentinel-2, and Hyperion (2) capacity to acquire regional perspectives of the vast regions (3) convenience in combining data from several sensors (4) no risk or difficulty in reaching distant places (5) coverage of a large range of energy ranges (e.g. UV, optical, infrared and so on) (6) availability of high-quality computer analysis software, and (7) efficient and cost-effective (Awawdeh et al., 2023). Remote sensing images are used as a common tool for land cover classification (Mercier et al., 2019). Observation, identification, mapping, and monitoring of land cover are immensely facilitated by remote sensing and digital image processing over a range of spatial, temporal, and thematic scales (Gómez et al., 2016). Remote sensors that operate on different physical principals to record land surface information can be categorized into optical, thermal, and RADAR sensors which make use of

reflected, emitted, and scattered energy respectively for data acquisition (Joshi et al., 2016). However, optical and radar-based remote sensing methods are most commonly used for land surface data collection. Though most of the existing studies use optical remote sensing data for land cover classification, it is difficult to perform this job with optical remote sensing data alone due to spectral confusion (Hu et al., 2021). The usefulness of SAR data, as a complementary source of information, is well reported because it is argued that the Synthetic Aperture Radar (SAR) data, which is sensitive to soil moisture and geometric configuration of the land surface, provides complementary information for optical remote sensing data, thus, offering an opportunity to be used in combination with optical data (Zhang, H. et al., 2015). The use of multisource data to improve land cover classification has become widespread (Sukawattanavijit et al., 2017), and aspects, like complementarity, interoperability, and synergetic strengths of different sensors, have been exploited by many researchers to achieve improved results in areas of land cover classification, identification of threats and environmental and crop monitoring (Sandberg, 2016). Several studies (De Alban et al., 2018; Laurin et al., 2012; Symeonakis et al., 2018; H. Zhang et al., 2015) have successfully employed the combined use of optical and SAR data to improve land cover classification accuracy.

Recently the European Space Agency has launched two new generation platforms that provide Sentinel-1 (C Band SAR) and Sentinel-2 (MSI) images. Unlike most SAR (Radarsat-2, ALOS-2, TerraSAR-X) and Optical data (GeoEye, Quickbird, IKONOS, SPOT, and Worldview), Sentinel-1 and Sentinel-2 images are available free of charge under an open license policy (Mercier et al., 2019). S2 has the potential for mapping six to twelve land cover classes, while using a single date image has been demonstrated by

some recent studies (Clark, 2017; Haas and Ban, 2018; Hdoush et al., 2022; Immitzer et al., 2016; Mongus and Žalik, 2018). The application of S1 has been mostly confined to its combined use with S2 or Landsat data for achieving increased classification accuracy (Inglada et al., 2016; Kussul et al., 2017; Laurin et al., 2022; Zhou et al., 2018). In several instances, the potential of integrated use of Sentinel-1 (SAR) and Sentinel-2 (Optical) data has been reported that included areas like LULC classification (Carrasco et al., 2019; Clerici et al., 2017; Dobrinić et al., 2020; Hu et al., 2021; Tavares et al., 2019), forest cover prediction (Heckel et al., 2020; Poortinga et al., 2019), vegetation species identification (Bjerreskov et al., 2021; Mendes et al., 2019; Zhang, H. et al., 2018), crops type mapping (Blickensdörfer et al., 2022; Cai et al., 2019; Orynbaikyzy et al., 2020; Van Tricht et al., 2018), and wildfire assessment (Colson et al., 2018).

Fusion of multiple data sources can be performed at three different levels: viz pixel level, feature level, and decision level fusion. Due to the presence of speckle noise, pixel-level fusion is not recommended for SAR images, and the use of feature-level fusion can help avoid this problem (Zhang, H. et al., 2015). Numerous applications (Mercier et al., 2019; Tavares et al., 2019; Van Tricht et al., 2018) reported that the fusion of data from Sentinel-1 and Sentinel-2 images increased the quality and accuracy of classification. It is advocated that Random Forest (RF) can outperform the traditional parametric approaches because of its ability to deal with noise and unbalanced datasets (Abdullah et al., 2019), and it can perform well when large datasets with many different features are involved (Belgiu & Drăguţ, 2016). This study involves feature-level image fusion and a random forest classification algorithm to carry out LULC classification of the study area.

Review of relevant literature reveals that most of the studies (Hussain et al., 2020; Majeed et al., 2021) in this country have used optical data for land cover classification. However, hardly few studies (Ali et al., 2018; Zahid Khalil and Saad-ul-Haque, 2018) can be found that focused on the use of SAR data for land cover classification, and only a very few cases involved the combined use of SAR and optical data in application areas like mapping of impervious surfaces (Shrestha et al., 2021) and crop types (Tufail et al., 2022). Land cover mapping through integrated use of SAR and optical data has been neglected so far from the study area perspective, and this gap has also been identified by Ali et al., 2018. This study is an attempt to explore the potential of Sentinel-1 SAR and Sentinel-2 optical data for land cover classification in the area of interest separately and combining data from both sources. The study may benefit resource managers and planners, especially when land use change reports are to be prepared for reporting purposes under the REDD+ mechanism that focuses on climate change mitigation endeavors across the globe including the study-focused region.

2. Materials

2.1 Study Area

The selected study area is located in Pakistan's administered part of the State of Jammu and Kashmir known as Azad Jammu & Kashmir (AJK). The State lies between 73-75^0 E and 33-36^0 N and occupies an area of 13297 km^2. It comprises 3 administrative divisions and 10 districts with a population of 4.179 million. The State falls in the Himalayan belt with mountainous topography in northern districts (Neelum, Muzaffarabad, Hattian, Bagh, Haveli, Poonch, and Sudhnuti) and relatively low hilly and undulating terrain of

southern districts (Kotli, Mirpur, and Bhimber). The chosen study area extent covers 2059 km^2. It mainly includes Poonch and Sudhnuti districts with a small portion of Bagh and Kotli districts (Figure 1). These districts lie almost at the center of the north-south projected map of the State and include representative land use land cover (LULC) types, such as water bodies, vegetation cover, settlements, bare soil, and grass. The area is characterized by a sub-tropical to temperate type of climate. Broadly, the area experiences four seasons: spring (March-April), summer (May-August), autumn (September-November), and winter (December-February). The area experiences a distinct rainfall pattern where most of the rain occurs in monsoon (July to September) with occasional winter showers (December to March). At high altitudes, most of the winter precipitation is received as snowfall whereas low-lying areas are showered with rain only. The average annual rainfall that occurred during the last 10 years ranges from 899 millimeters to 1132 millimeters. Rawalakot and Bagh Districts experience relatively cooler surface temperatures compared to the Sudhnutii and Kotli Districts. The average surface temperature recorded for the winter and summer seasons is 9.05^0C and 23.64^0C respectively. The maximum temperature spikes as high as 38.02^0C while the minimum temperature drops as low as -4.11^0C (Source: https://chrsdata.eng.uci.edu/)

Topography is mainly hilly where the slope varies from 0 to 57 degrees with rugged terrain on hill slopes and relatively plain valley stretches. The elevation range of the area stretches from 372 m to 3384 m above mean sea level (msl) where microclimate varies with altitude and sets conditions for vegetation of different types. Figure 2 characterizes the topography of the study area. Landscape portrays a mixture of different land use land cover (LULC) types where settlements, water channels, and bare soil, with fragmented

patches of forest, are the most prominent features. The population of the two main districts (Poonch and Sudhnuti) is 0.818 million (PNDD, 2015). Since the area has been enjoying fast infrastructural development for the last two decades. Therefore, LULC is also changing rapidly with developmental processes where increasing population causes a notable change in built-up areas and natural as well as planted vegetation cover. The main forest types of the area include Subtropical Chir Pine, Moist Temperate Conifers, and Scrub Forests. However, forest cover is predominantly occupied by Subtropical Chir Pine forest with Chir pine *(Pinus roxburghii) as* a typical species. Major species of the Moist Temperate Coniferous forest are blue pine (Pinus wallichana) and a few mixed broadleaved species. Scrub forest type is mainly dominated by wild olive *(Olea cuspidata)* and hop-bushes *(Dedonia viscosa)*. As local communities are allowed to collect fuel wood and fodder from these forests and in addition to these rights, they are also entitled to grant of timber needed for house construction. Therefore, the heavy dependence on surrounding communities tends to increase pressure on forest resources, thereby aggravating the common environmental problems like deforestation, destruction of wildlife habitat, and landslides. Small average land holdings and scarcity of cultivable land restrict agriculture to narrow terraced land developed around houses on steep mountain slopes. Maize and wheat are the major agricultural products, whereas livestock rearing is also practiced at a limited scale to cater to household dairy needs.

Article in Press: JJEES 16(2), June 2025.
This article has been accepted for publication and will appear in the upcoming issue. The final published version will be available through the journal website after copyediting, typesetting and proofreading. ©2025 JJEES.

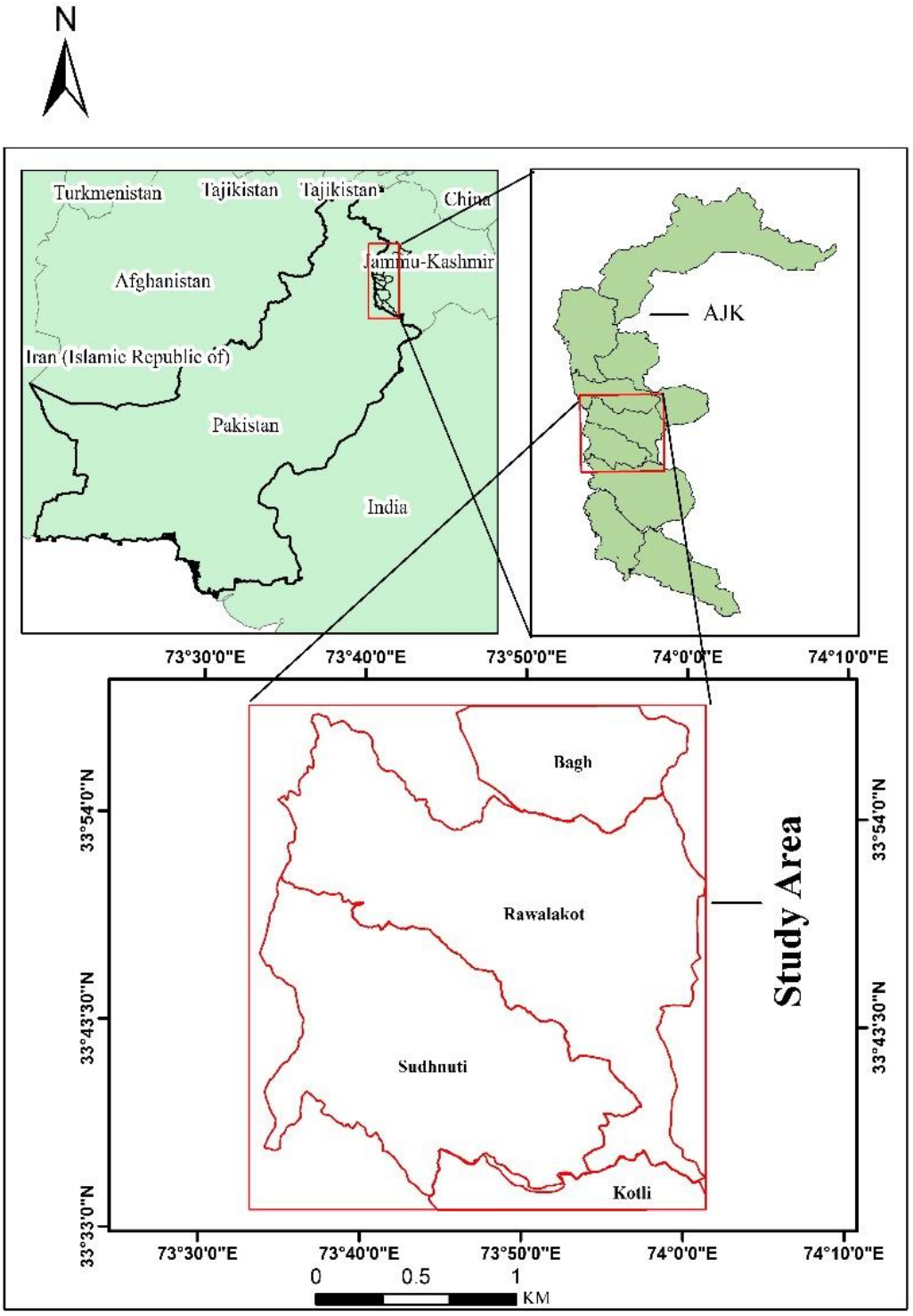

Figure 1: Study area map

Article in Press: JJEES 16(2), June 2025.
This article has been accepted for publication and will appear in the upcoming issue. The final published version will be available through the journal website after copyediting, typesetting and proofreading. ©2025 JJEES.

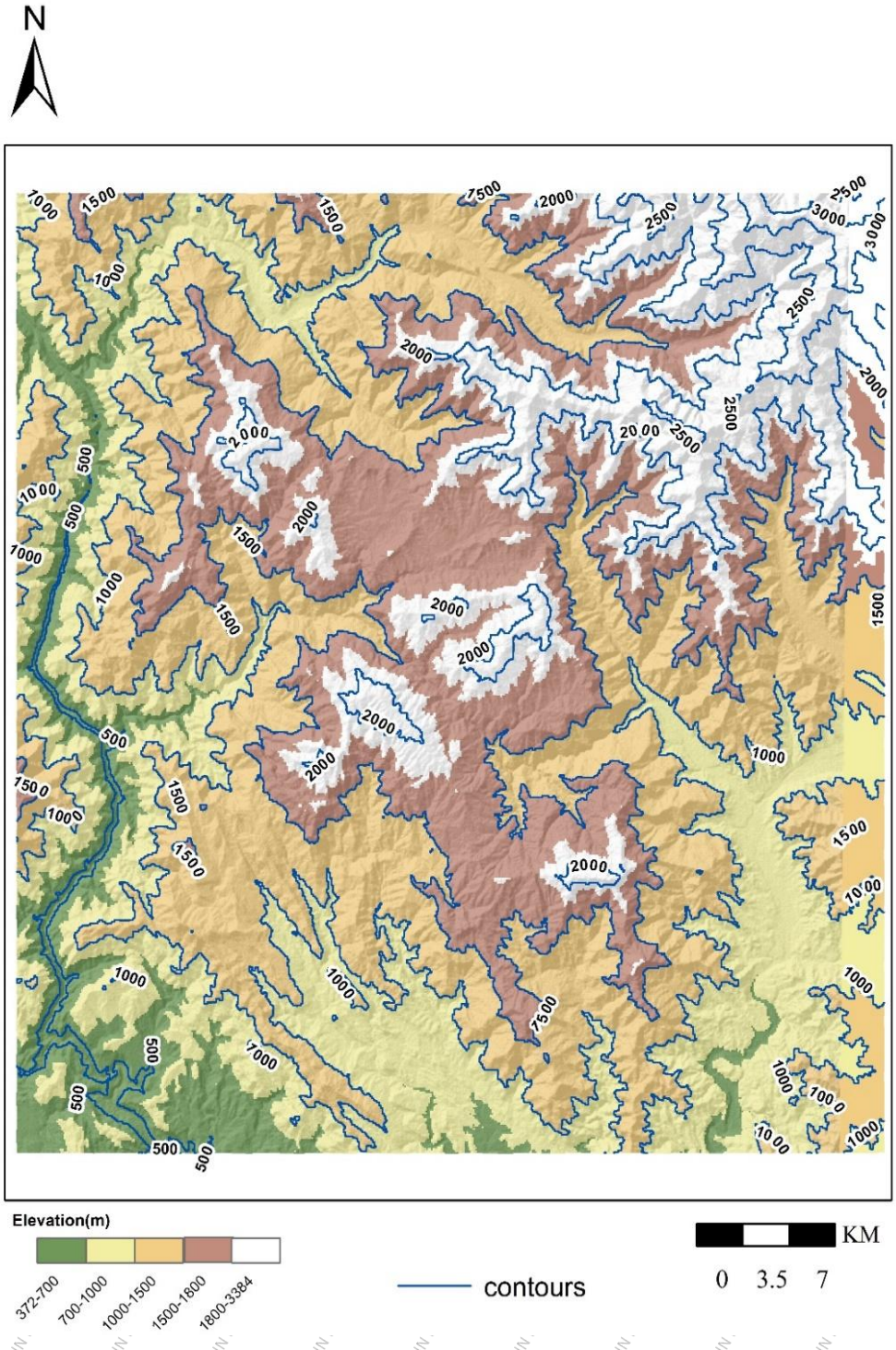

Figure 2: A DEM depicting topography of the study area

Article in Press: JJEES 16(2), June 2025.
This article has been accepted for publication and will appear in the upcoming issue. The final published version will be available through the journal website after copyediting, typesetting and proofreading. ©2025 JJEES.

2.2 Satellite Data

Using satellite imagery, detection, and mapping of land cover involves a number of steps that include selection of required sensor data, definition of land cover classes, data processing and feature extraction, preparation of input datasets for classification, decision of an appropriate classification method, and analysis of outputs.

Satellite data from Sentinel-1 (SAR) and Sentinel-2 (Optical) sensors were employed for land cover classification in the area of interest (AOI). The Sentinel data were downloaded from the official website (http://scihub.copernicus.eu./dhus/≠/home) available via the Copernicus Open Access Hub of the European Space Agency (ESA). Both Sentinel-1 and Sentinel-2 images were collected in Level 1 format which needed several preprocessing steps before use for further analysis.

2.2.1 Sentinel-1 (S1) SAR image

Sentinel 1 Synthetic Aperture Radar (SAR) mission is comprised of 1A and 1B polar-orbiting satellites. The European Space Agency (ESA) launched Sentinel 1A in April 2014 which was followed by Sentinel 1B in April 2016. The data captured in the 'C' band is delivered with dual polarization, i.e. Vertical-Horizontal (VH) and Vertical–Vertical (VV). The products that are suitable for Level-0, Level-1, and Level-2 processing are provided in three different operational modes known as Interferometry Wide Swath (IW), Strip map (SM), and Extra Wide Swath (EW). The Synthetic Aperture Radar imaging is carried out with a repeat cycle of 6 days (Liu et al., 2018). Sentinel 1 (S1) data is available free of charge for different applications under the open data license policy of ESA. A

Ground Range Detected (GRD) S1 Level-1 product recorded in Interferometry Wide Swath (IW) mode, acquired on September 23, 2020, was downloaded for the study.

2.2.2 Sentinel-2 (S2) Optical Image

The Sentinel-2 (S2) is a high-resolution, wide-swath multi-spectral imaging mission. It comprises 2A and 2B satellites that were launched by the European Space Agency (ESA) in 2015 and 2017 respectively. A state-of-the-art multispectral imaging instrument (MSI), carried by Sentinel-2A, captures the data in 13 spectral bands with 10 m (four bands), 20 m (six bands), and 60 m (three bands) spatial resolution. A Sentinel 2A Level 1C multispectral image, acquired on September 17, 2020, corresponding to the study area, was downloaded for this study.

2.2.3 Multi-Sensor Dataset

Apart from S1 and S2-derived datasets, a third type of multi-sensor (S1+S2) dataset was also prepared to be exploited for land cover classification. The SAR VH, VV channels, and SAR-derived texture images were resampled to 20 m using the nearest neighbor resampling method, so that they are compatible with stacking with S2A spectral bands and indices of 20 m spatial resolution. A separate dataset, consisting of four 10 m spatial resolution S2A spectral bands in combination with SAR VH, VV images, and SAR-based textures with their original resolution of 10 m, was also generated to be used for LULC classification. Image stacks, consisting of S2 and S1-derived features, were prepared in QGIS.

2.4 Reference Data

The dominant representative land use land cover classes of the area were considered for classification. Among these LULC types, water, vegetation, settlements, bare soil, and grasses are the key categories that were taken into account for detection and mapping purposes. Training samples of six land cover classes namely water, mixed forest, shrublands, bare soil, built-up area and grassland were selected based on knowledge of the area on high-resolution Google Image of the study site. Table 1 provides the description of land use/land cover classes and selected training samples.

3. Methods

3.1 Pre-processing of S1 (SAR) Image

The preprocessing steps included calibration, speckle filtering, terrain correction, sub-setting, and image export. Sentinel 1 Level-1 products are not radiometrically corrected, therefore, calibration is required for the transformation of pixel values from simple digital numbers to SAR backscatter. Radiometric calibration was performed as the first step by calculating the sigma nought for the given image. Image calibration was followed by speckle filtering that was intended to remove speckle noise in the image. A Lee speckle filter with 3x3 windows was applied for speckle suppression that resulting in the production of a relatively smoother image. Since geometric distortions are inherently found in Level-1GRD images, geometric correction was also a necessary step. Range Doppler Terrain correction was applied to convert the image into a map system that was projected into WGS84 UTM Zone 43 N. Generally, it is easier to work with the image in decibel (db) format; therefore, the image was transformed from linear to db units. Finally, the image was subset to the desired extent of the study area with a 10 m pixel size. All

these SAR image preprocessing steps were performed in SNAP 8.0 open-source software. A third band (VV-VH) was also produced from VH and VV polarization channels since this band combination is considered optimal for land cover classification (Abdikan et al., 2016).

Textural information of a satellite image is of foremost importance in land cover mapping (Sylla et al., 2021). SAR texture measures are recognized as a valuable source of information and it is believed that SAR textures may serve as a useful input for land cover classification because single pixel values in SAR imagery are not reliable due to inherent speckle noise (Zhu et al., 2012). Many methods and techniques have been developed for the calculation of image textures. However, among previously proposed methods, the Grey Level Co-occurrence Matrix (GLCM) approach is considered one of the most reliable statistical methods used for derivation of textures from a satellite image (Zakeri et al., 2017). In this study, the most commonly used texture measures were extracted for LULC mapping using the GLCM approach introduced by Haralick et al., 1973. These included Angular Second Moment (ASM), Contrast (CON), Dissimilarity (DIS), Homogeneity (HOM), Entropy (ENT), Mean (AVG), and Variance (VAR). Generally, image textures are worked out by considering a moving window of a specific size that performs some mathematical calculation around a pixel of interest (Kavitha et al., 2021). SAR textures were calculated for both VH and VV polarizations in SNAP software using window sizes of 7x7, 9x9, and 11x11, and different combinations of derived textures were used as input variables for classification.

3.2 Pre-Processing of Optical (S2) Image

The Sentinel-2A L1C provides top-of-atmosphere (TOA) reflectance, and the wavelengths of image bands range from 443 nm to 2190 nm. The downloaded S2 L1C tile was atmospherically corrected to obtain surface reflectance using the Sen2Cor application integrated with SNAP. The image was transformed from L1C to L2A and only the bands with 10 m spatial resolution (B2, B3, B4 & B8) and 20 m (B2, B3, B4, B5, B6, B7, B8A, B11 & B12) were used for further analysis with their original resolutions, whereas bands with 60 m spatial resolution were excluded for further consideration. These atmospherically corrected spectral bands were clipped to the study area extent and made ready for stacking and calculation of spectral indices. In addition to individual spectral bands, five indices (NDVI48, NDVI48a, NDVI56, NDVI57, and NDVI68a) were also calculated, using different combinations of spectral bands and included in the datasets prepared for land cover classification. Composites of S2A 20 m & 10 m spatial resolution spectral bands and calculated indices were produced, using different combinations, and an input dataset was prepared for categorization of images into predefined land cover classes. A description of land use /land cover classes of the study area and samples selected for classification purposes is provided in Table 1.

Table 1: A description of land use /land cover classes and samples selected for classification purpose

Sr No	Land Cover Class	Description of Class	No of Polygons	No of Pixels
1	Water	River, secondary, and tertiary water streams	8	894
2	Mixed Forest	Managed and unmanaged forest cover comprising predominantly of conifers with a mix of broadleaved trees	42	19746
3	Shrubland	Scrub forest inhabiting shrubby vegetation, short-statured woody and herbaceous flora	45	4254
4	Bare Soil	Bare land, sparsely vegetated areas with dominant soil background, exposed substrata due to landslides, ploughed terraces yet not cultivated, mud houses, and earthen roads	78	633
5	Built-Up	Settlements, manmade artificial structures, cemented and asphalt roads, rocks and boulders	69	1748
6	Grassland	Forest floor covered with grasses and herbs in open	31	1764

Article in Press: JJEES 16(2), June 2025.
This article has been accepted for publication and will appear in the upcoming issue. The final published version will be available through the journal website after copyediting, typesetting and proofreading. ©2025 JJEES.

	canopy forest, Grass covered farmlands, meadows, and grassy hill slopes

3.3 Land Cover Classification

Land cover types, corresponding to pixel values of a satellite image, are extracted by means of a widely used method called image classification (Orlíková and Horák, 2019).

Satellite image classification has been carried out using numerous image classification techniques that can be grouped into different categories (Chowdhury, 2024). In recent years, the use of machine-learning algorithms has attracted a considerable amount of attention for LULC mapping while employing remotely sensed imageries (Adam et al., 2014; Maxwell et al., 2019). It is believed that machine-learning algorithms are more accurate and noise-resistant than common algorithms (Rodriguez-Galiano, V. F. et al., 2012). As far as LULC studies are concerned a machine learning algorithm that was introduced by Leo (Breiman, 2001) in 2001 known as random forest (RF) is deemed to be the most suitable model for land cover classification (Gislason et al., 2006; Guo et al., 2011).

Currently, when it comes to remote sensing data, RF is reckoned to be the most widely used algorithm for land cover classification (Amani et al., 2019; Cánovas-García et al., 2017; Kelley et al., 2018; Maxwell et al., 2019; Millard and Richardson, 2015; Teluguntla et al., 2018). According to Mahdianpari et al. (2017) and Xia et al. (2017) the key reasons for which the RF received considerable approval over the last two decades include (i) good handling of outliers and noisier datasets (ii) good performance with high

dimensional and multi-source datasets (iii) higher accuracy than other popular classifiers, such as SVM, kNN or MLC in many applications (Abdel-Rahman et al., 2014; Rodriguez-Galiano, Victor F. and Chica-Rivas, 2014) and (iv) increasing the processing speed by selecting important variables (Van Beijma et al., 2014). In addition to this, the requirement of only two parameters (ntree and mtry) that need to be optimized is another prominent factor that makes RF more acceptable than other machine learning algorithms (like SVM) since it facilitates the application of RF (Maxwell et al., 2018). Many studies (Abdel-Rahman et al., 2014; Praticò et al., 2021; Rodriguez-Galiano, V. F. et al., 2012) have proved that this approach achieved the best results as compared to other classification algorithms such as SVM, MLC, kNN, and CART.

In this study, the Random Forest algorithm was chosen for land cover classification because previous research shows that RF performed excellently in classifying diverse remote sensing datasets (Gislason et al., 2006; Rodriguez-Galiano, V. F. et al., 2012) especially, when optical and radar data were used as combined datasets. It has been inferred that LULC classification accuracy can be improved effectively employing the fusion of optical and SAR images. Currently, three levels of image fusion are generally practiced in remote sensing. These methods include (i) pixel level (ii) feature level and (iii) decision-level image fusion. Since feature-level fusion takes into account factors, like feature information and correlation contained in the image itself, and obtains more macro-level feature-level information, therefore, it has been revealed that feature-level image fusion is considered a more appropriate technique than pixel pixel-level approach (Zhang, R. et al., 2020). Feature-level image fusion method was used in this study that involves the application of feature stacking. Image stacks of S1 & S2 derived features

Article in Press: JJEES 16(2), June 2025.
This article has been accepted for publication and will appear in the upcoming issue. The final published version will be available through the journal website after copyediting, typesetting and proofreading. ©2025 JJEES.

were used as predictors for land cover classification. Input datasets for land cover classification contained diverse composites that were prepared from different S1 (SAR) and S2 (Optical) derived features. These datasets were generated separately from extracted variables of S1 and S2 images as well as band stacks were also produced by combining feature layers from both sources (S1+S2). The number of trees was set to 100 because it helps reduce time without causing any notable loss in accuracy (Mercier et al., 2019). The prepared set of training samples was used with a 50/50 ratio (Training and Validation). Figure 3 illustrates the spectral reflectance curves of LULC classes sampled for classification purpose. Different types of datasets based on S1 & S2 derived

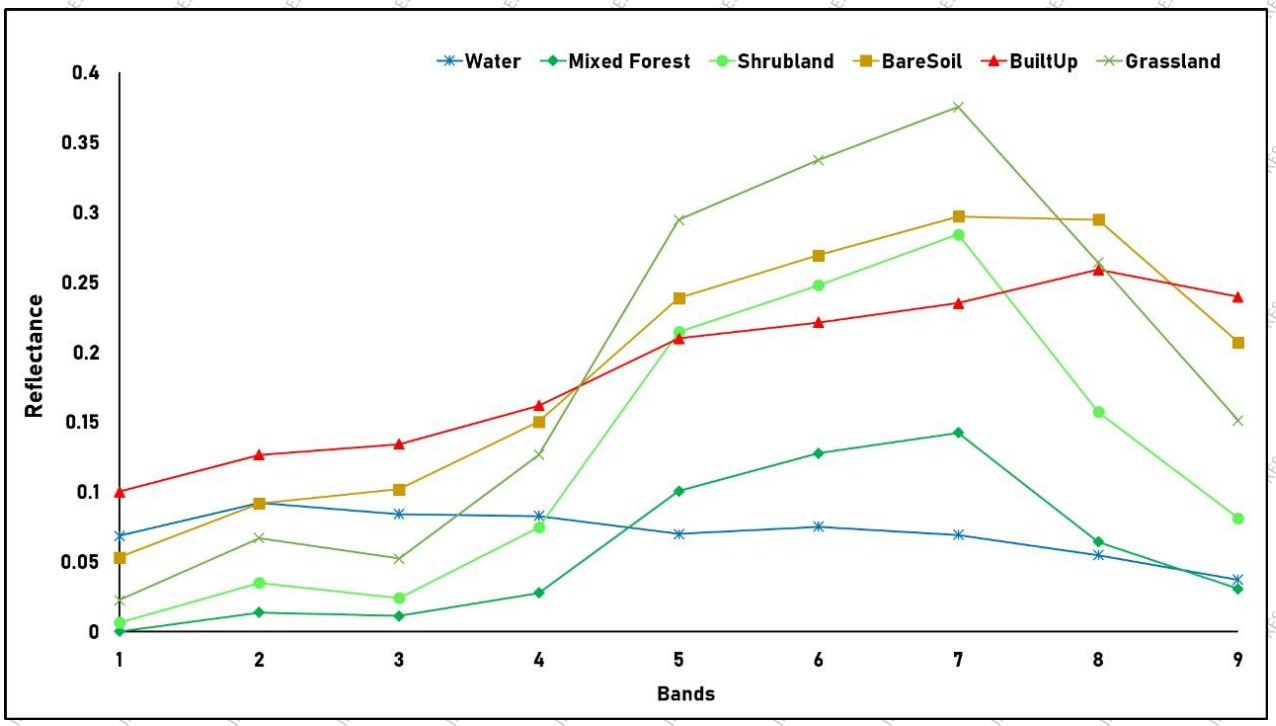

Figure 3: Reflectance spectra of LULC classes utilized for classification purposes.

features/variables (S1-alone, S2-alone, S1+S2 combined) were used for LULC classification (Table 2), and each classification scenario was examined to analyze the classification accuracy (Table 3). An error matrix with an equal number of rows and

columns expresses the relationship between classification and validation data and is generally used as a standard to measure classification accuracy (Orlíková and Horák, 2019). Therefore, an error matrix was used to calculate the overall accuracy (OA), User accuracy (UA), and Producer accuracy (PA). The flow of the classification process is illustrated in Figure 4. Random Forest land cover classification was executed in Orfeo Toolbox integrated with QGIS open source software, whereas Arc-GIS and Arc-GIS Pro were used for map layout and extraction of spectral reflectance curves.

Article in Press: JJEES 16(2), June 2025.
This article has been accepted for publication and will appear in the upcoming issue. The final published version will be available through the journal website after copyediting, typesetting and proofreading. ©2025 JJEES.

Table 2 shows different scenarios of RF-based LULC classification carried out using different combinations of S1 & S2 derived variables

Classification Scenario	Datasets	No of variables
	Sentinel-1 Based Datasets	
1	VH, VV, (VV-VH)	3
2	VHVV_11, (VH, VV)	16
3	VHVV_79, (VH, VV)	30
4	VH_7, VV_11, (VH, VV)	16
5	VH_11, VV_9, (VH, VV)	16
6	VH_7911, (VH, VV)	22
7	VV_7911, (VH, VV)	22
8	VH_7, (VH)	8
9	VH_11, (VH)	8
10	VV_7	7
11	VH_9	7
12	VV_9	7
13	VH_11	7
14	VH_9, VV_7	14
15	VV_9, (VH, VV)	9
Sentinel-2 Based Datasets		
1	B2, B3, B4, B5, B6, B7, B8A, B11, B12	9
2	B2, B3, B4, B5, B6, B7, B8A, B11, B12 and indices (NDVI48, NDVI48a, NDVI56, NDVI57, NDVI68a)	14
3	B2, B3, B4, B8	4
4	B2, B3, B4, B8 and NDVI	5
S1+S2 combination Based Datasets		
1	B2, B3, B4, B5, B6, B7, B8A, B11, B12 and VHVV_11 (VH, VV)	25
2	B2, B3, B4, B5, B6, B7, B8A, B11, B12 and indices (NDVI48, NDVI48a, NDVI56, NDVI57, NDVI68a) and VHVV_11, (VH, VV)	30
3	S2 indices and VHVV_11, (VH, VV)	21
4	B2, B3, B4, B8 and VHVV_11, (VH, VV)	20
5	B2, B3, B4, B5, B6, B7, B8A, B11, B12 and VH_7, VV_11, (VH, VV)	25
6	B2, B3, B4, B5, B6, B7, B8A, B11, B12, S2 derived indices (NDVI48, NDVI48a, NDVI56, NDVI57, NDVI68a) and VH_7, VV_11 (HV, VV)	30
7	B2, B3, B4, B8, and VH_7, VV_9, (HV, VV)	20

Note: SAR: VH, VV refer to SAR polarization images, VH_a, VV_b denote the VH, VV derived SAR textures with respective window size,
Optical: B1, B2 …. Refer to spectral band number of S2 image, NDVI = Normalized Difference Vegetation Index and ab denote the spectral bands used for derivation of a specific index

Table 3 shows different scenarios of random forest classification with S1 & S2 derived set of variables and their associated overall accuracy and Kappa Coefficient value.

Classification Scenario	Sentinel-1 Based Datasets	Kappa Index Value	Overall Accuracy (OA%)
1	VH, VV, (VV-VH)	0.33	44.65
2	VHVV_11, (HV, VV)	0.55	63
3	VHVV_79 (HV, VV)	0.53	61
4	VH_7VV_11, (HV, VV)	0.53	61
5	VH_11, VV_9, (HV, VV)	0.51	59.84
6	VH_7911, (HV, VV)	0.52	60
7	VV_7911, (HV, VV)	0.43	52.91
8	VH_7, VH	0.35	47.93
9	VH_11, VH	0.52	60
10	VV_7	0.33	44.65
11	VH_9	0.41	50.95
12	VV_9	0.32	43.86
13	VH_11	0.52	60
14	VH_9, VV_7	0.50	59
15	VV_9, (VH, VV)	0.42	52

Article in Press: JJEES 16(2), June 2025.
This article has been accepted for publication and will appear in the upcoming issue. The final published version will be available through the journal website after copyediting, typesetting and proofreading. ©2025 JJEES.

	Sentinel-2 Based Datasets		
1	B2, B3, B4, B5, B6, B7, B8A, B11, B12	0.85	88.12
2	B2, B3, B4, B5, B6, B7, B8A, B11, B12 and indices	0.87	89.59
3	B2, B3, B4, B8	0.83	86
4	B2, B3, B4, B8 and NDVI	0.84	87
	Sentinel-1 & Sentinel-2 (S1+S2) Based Datasets		
1	B2, B3, B4, B5, B6, B7, B8A, B11, B12 and HVVV11 (HV, VV)	0.90	91.87
2	B2, B3, B4, B5, B6, B7, B8A, B11, B12 and indices and VHVV_11 (VH, VV)	0.91	93.12
3	S2 indices and VHVV_11 (VH, VV)	0.74	79
4	B2, B3, B4, B8 and VHVV_11 (VH, VV)	0.84	87
5	B2, B3, B4, B8, NDVI and VHVV_11 (VH, VV)	0.86	88.57
6	B2, B3, B4, B5, B6, B7, B8A, B11, B12 and VH_7, VV_11, (HV, VV)	0.87	89
7	B2, B3, B4, B5, B6, B7, B8A, B11, B12, S2 derived indices (NDVI48, NDVI48a, NDVI56, NDVI57, NDVI68a) and VH_7, VV_11, (HV, VV)	0.87	89
8	B2, B3, B4, B8, and VH7VV9 (HV, VV)	0.83	86

Article in Press: JJEES 16(2), June 2025.
This article has been accepted for publication and will appear in the upcoming issue. The final published version will be available through the journal website after copyediting, typesetting and proofreading. ©2025 JJEES.

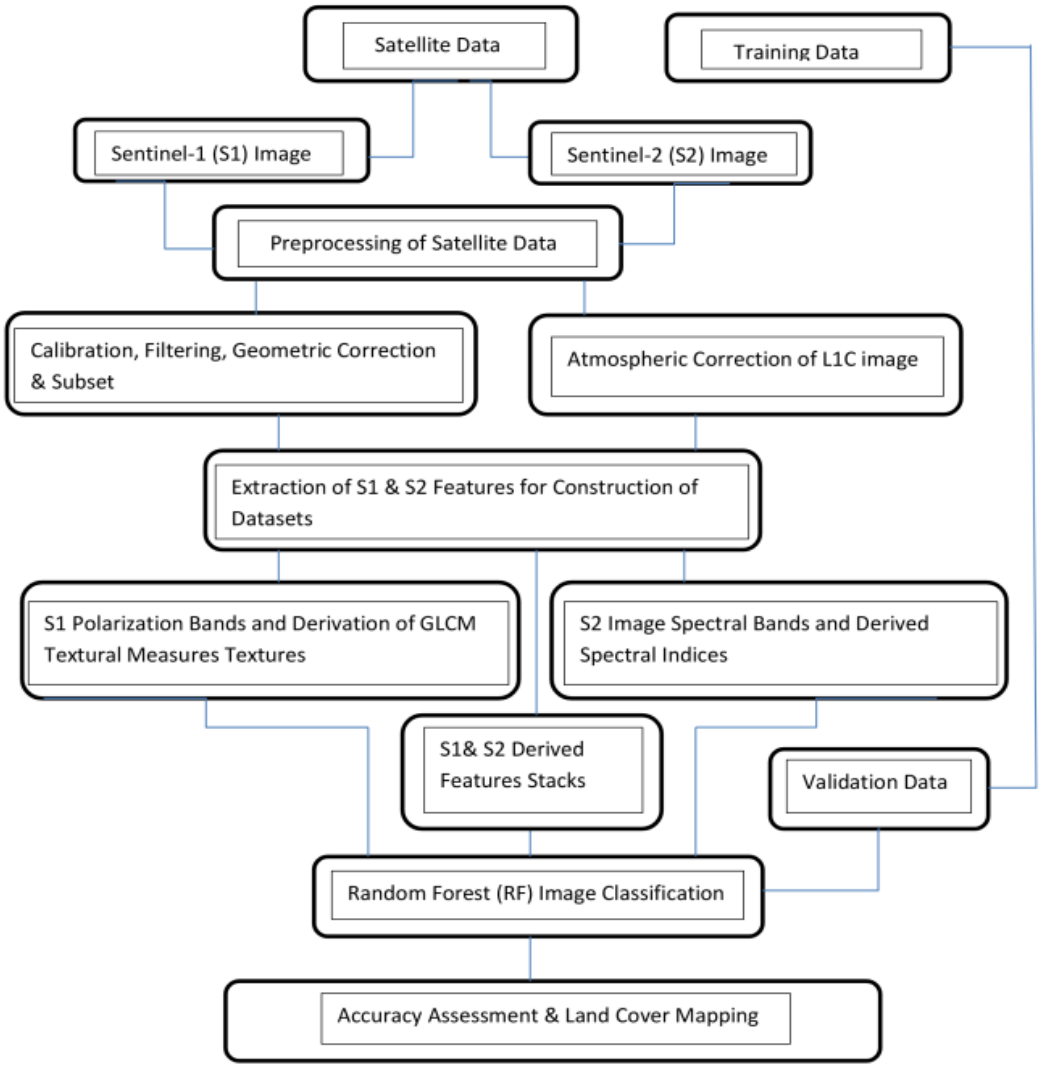

Figure 4: Diagram depicting flow of work

Article in Press: JJEES 16(2), June 2025.
This article has been accepted for publication and will appear in the upcoming issue. The final published version will be available through the journal website after copyediting, typesetting and proofreading. ©2025 JJEES.

4. Results

Firstly, the image composites, produced from SAR VH, and VV polarizations, were used alone for land cover classification employing a random forest classifier. The image, consisting of VH-VV, and VV-VH polarimetric channels, produced an overall (OA) accuracy of 44.65% and a Kappa coefficient (KC) of 0.33. Afterward, different combinations of SAR-based datasets consisting of SAR textures (derived with varying window sizes of 7x7, 9x9, and 11x11) either alone or combined with SAR VH, and VV polarizations were exploited for classification purposes. These combinations presented different degrees of accuracy for land cover classification. Among the given S1- -alone datasets, a 16-layered image consisting of VH and VV polarization bands and derived SAR textures having window size 11x11 (denoted as VHVV_11) yielded the highest overall accuracy and Kappa coefficient (63.01%; KC= 0.55). Classification accuracy yielded by different combinations of Optical-SAR datasets with associated Kappa Index is furnished in Table 3.

Similarly, in optical domain band composites of S2A, spectral bands (20 m and 10 m spatial resolution) and derived spectral indices were analyzed for land cover classification. Individually, the band composite, consisting of B2, B3, B4, B5, B6, B7, B8A, B11, and B12 yielded overall accuracy and Kappa value of 88.12 % and 0.85 respectively whereas the highest overall accuracy of 89.58% with kappa statistics of 0.87 was recorded when nine layers of spectral bands were tried in combination with derived spectral indices. A dataset containing four spectral bands (10 m resolution) gave 86.34% OA (KC= 0.83) and the addition of the NDVI layer to this set of variables led to an increase in OA of 87.40 (KC= 0.84).

Article in Press: JJEES 16(2), June 2025.
This article has been accepted for publication and will appear in the upcoming issue. The final published version will be available through the journal website after copyediting, typesetting and proofreading. ©2025 JJEES.

The third type of dataset, used for RF-based LULC classification, consisted of features from both S1A and S2A images. Several image stacks were structured by combining data from Sentinel-1 and Sentinel-2 sources and employed to extract six predefined land cover classes using an RF classifier. The results provided different levels of accuracy. Out of the tested range of multiple combinations a thirty (30) layered feature stack developed by integrating SAR VH, VV polarizations, textures (ASM, Contrast, Dissimilarity, Homogeneity, Entropy, Mean and Variance derived from HV, VV polarizations using window size of 11x11), S2 spectral bands (B2, B3, B4, B5, B6, B7, B8A, B11 & B12) and spectral indices (NDVI48, NDVI48a, NDVI56, NDVI57, NDVI68a) produced highest overall accuracy of 93.12% and kappa coefficient value of 0.91. The indicated dataset (S1+S2 integrated features stack) proved to be the best combination among all of the datasets employed for the LULC classification of the study area. Table 3 shows different scenarios of the datasets that were used for LULC classification and their results in terms of overall accuracy and kappa coefficient. Error matrix (Table 4) demonstrates the overall accuracy (OA), Producer's accuracy, User's accuracy, and Kappa Coefficient (KC) value for the best-performing model. Figure 5 shows the classified image next to the Sentinel-2 natural color image whereas Figure 6 highlights the classified and reference land cover classes from the study area.

Table 4: Confusion matrix portraying accuracy statistics for best-performing combination of variables derived from SAR and Optical satellite data

		Reference						
	LC Classes	**Water**	**Mixed Forest**	**Shrublands**	**Bare Soil**	**Built-Up**	**Grasses**	**User's Accuracy**
Mapped	Water	77	0	0	1	2	0	0.96
	Mixed Forest	0	74	6	0	0	0	0.92
	Scrubland	0	4	73	1	0	2	0.91
	Bare Soil	1	0	5	68	3	3	0.85
	Built-Up	0	0	0	0	80	0	1

Article in Press: JJEES 16(2), June 2025.
This article has been accepted for publication and will appear in the upcoming issue. The final published version will be available through the journal website after copyediting, typesetting and proofreading. ©2025 JJEES.

	Grasses	0	0	5	0	0	75	0.93
	Producer's Accuracy	0.98	0.94	0.82	0.97	0.94	0.93	
	Overall Accuracy= 93% Kappa Index= 0.91							

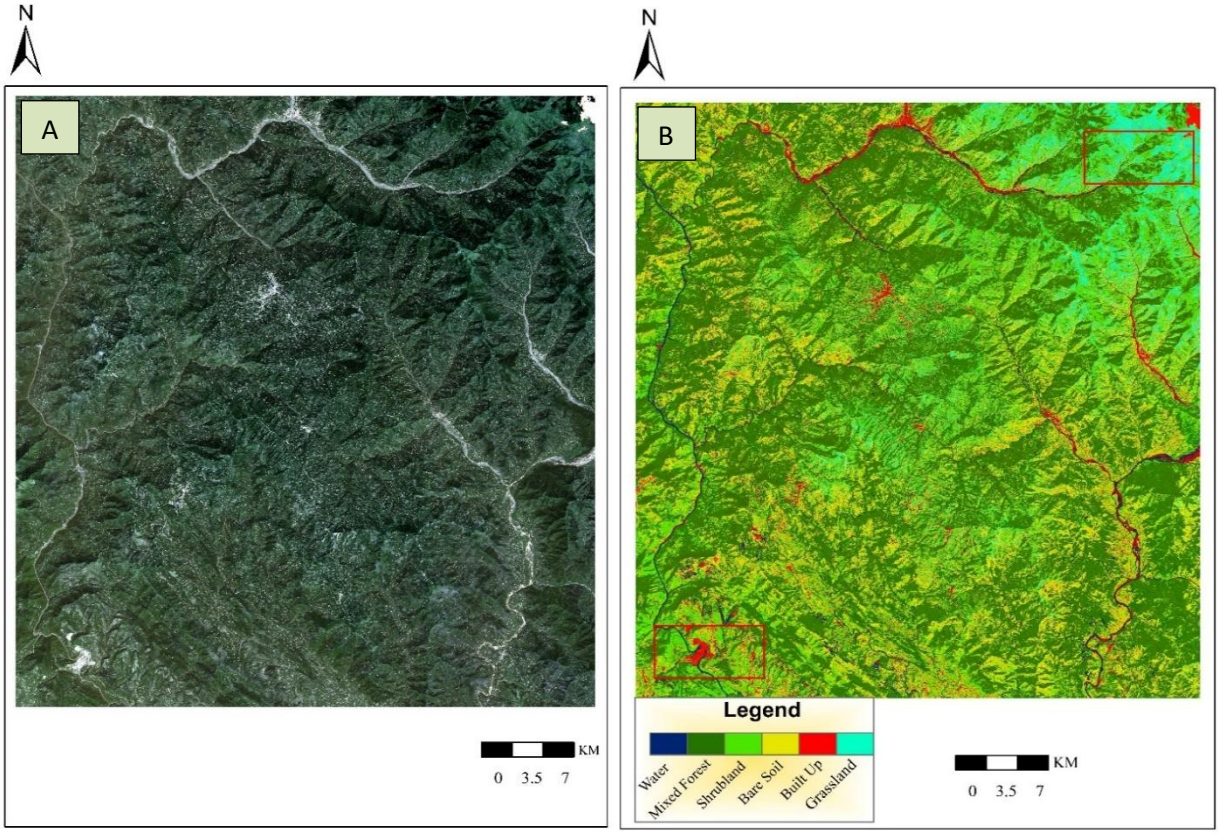

Figure 5: (A) Sentinel-2 natural colour image (B) A final LULC map obtained from combined use of Sentinel-1 and Sentinel-2 (S1+S2) derived features. Sections marked with red boxes highlight the

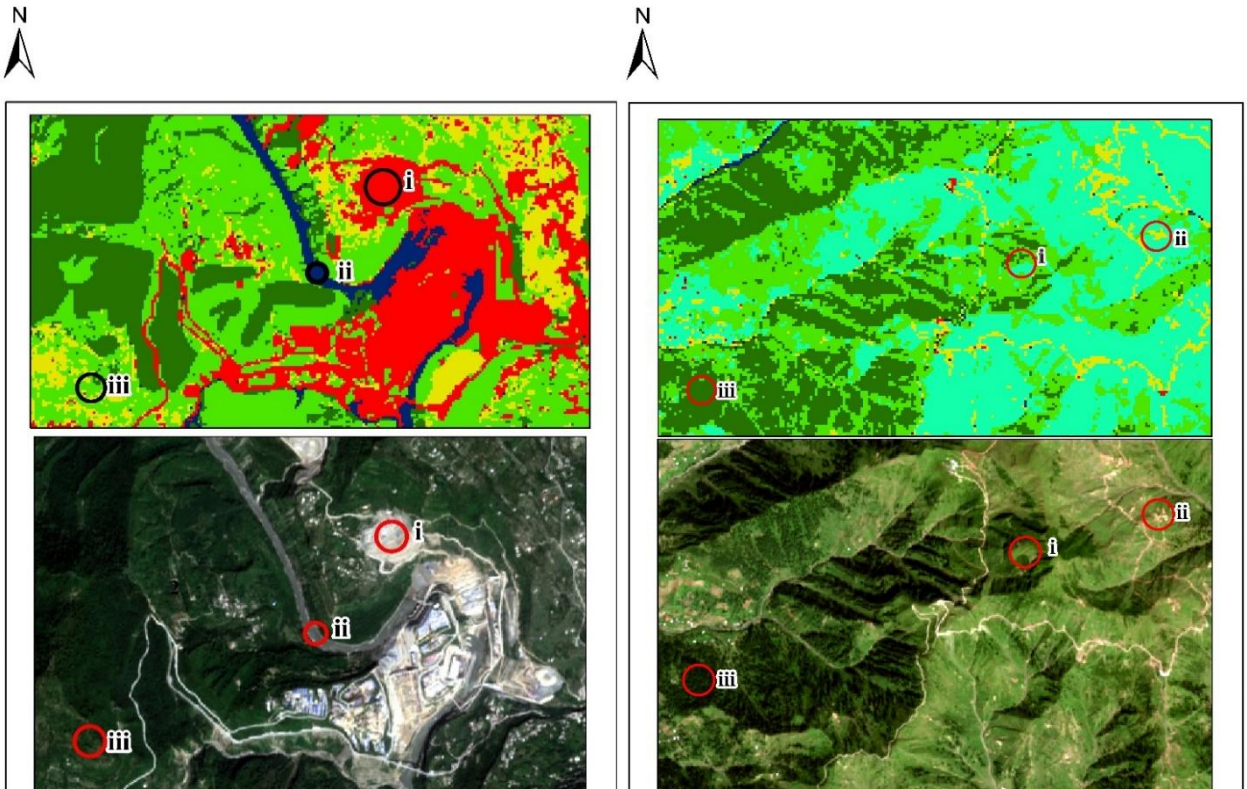

5. Discussion

Several studies have involved the integrated use of RADAR and optical data for land use land cover classification in different parts of the world and they have reported different levels of contribution from these two different data types in classification success both in their individual as well as in combined capacity. In this study, Sentinel-1 derived data set consisting of VH-VV and VV-VH variables produced an overall accuracy of 44.65% where the Kappa coefficient was 0.33. Our results are in line with some of the recently conducted studies that used Sentinel-1 data for land cover classification. For instance, Clerici et al. (2017) achieved only 20.12% overall accuracy with the Random Forest method where a Sentinel-1 image of the study area (in Colombia) was categorized into six LULC types. In another case, Mendes et al. (2019) applied RF to map vegetation types with Sentinel-1 scene in Mato Grasso, Brazil and reported an overall accuracy and kappa coefficient range of 45.51%-56.21% and 0.31-0.42 respectively. In the Moravian-Silesian region of the Czech Republic Orlíková and Horák (2019) categorized the S1 imagery into three land cover classes (Arable land, Grasses, and vine orchids) and indicated an overall accuracy of 46.28% and 61.5% for pixel-based classification that was performed at two different selected sites. Similarly, Nuthammachot and Stratoulias (2019) investigated the potential of the S1 image to classify five land cover classes across an area chosen in Thailand. They achieved an overall accuracy of 58.50% with a 0.48 Kappa coefficient value and the authors have reasoned that the SAR image was not able to clearly extract the pre-defined land cover classes except water and misclassification was more evident in forest and urban land cover classes. The study underlined that classification confusion was more pronounced in hilly parts of the selected site.

It has been learned that SAR textures help improve classification accuracy (Zhu et al., 2012). The inclusion of SAR textures significantly improved the classification accuracy in our case. We tried different combinations of SAR VH, VV polarizations, and 7 texture measures (ASM, Contrast, Dissimilarity, Homogeneity, Entropy, Mean, and Variance) that were derived, using windows of different sizes (7x7, 9x9, 11x11). These combinations produced results with varying ranges of overall accuracy and Kappa coefficient. Among the employed combinations, the lowest OA of 47.93% (Kappa statistic 0.35) was noted for a set of eight variables that contained VH polarization and seven texture measures (window size 7x7), whereas the highest OA (63.01%; Kappa value 0.55) was given by a dataset (consisting of 16 variables) that was developed by combining VH, VV polarization with their respective textures features (7 each) that were extracted using window size of 11x11. Datasets, consisting exclusively of SAR textures excluding polarization layers, were also examined for land cover classification, and different results were achieved for these applications. Amongst the textures derived from a single polarization band VV based textures (7x7 window size) yielded the lowest accuracy (OA= 44.65, Kappa Coefficient= 0.33), whereas VH-associated textures (window size of 11x11) generated the best results (OA= 60.37, Kappa Coefficient= 0.52). SAR dataset created merely from backscattering components produced low producer's and user's accuracies (34% and 22%) for the shrubland but these accuracies started improving with the introduction of SAR textures and increased up to 61% and 34% with VHVV_11. Different combinations of SAR polarizations and texture variables with corresponding OA accuracy and Kappa values have been shown in Table 3. Results of our study about the role of Sentinel-1 derived textures in LULC classification are supported by several studies where GLCM SAR textures proved useful towards

improving LULC classification accuracy. This refers to Tavares et al. 2019 where the study attempted to extract 12 land cover classes in Brazil employing Random Forest (RF) classifier and obtained 56.01% (KC=0.41) overall accuracy while using Sentinel-1 data alone but the classification accuracy increased to 61.61% (KC=0.48) when SAR textures were also combined with Sentinel-1 data. In another example, Zakeri et al. (2017) performed a land cover classification task in Tehran (Iran) while using SAR backscatter data and SAR textures and it was revealed that Sentinel-1 textures performed better than Sentinel-1 backscatter-only scenarios. When GLCM-based Sentinel-1 textures (window size 11x11) were included for LULC classification the OA accuracy increased from 45.7% to 54.2% with respective increase in kappa coefficient from 0.29 to 0.41. It was reported by Inglada et al. (2016) that Sentinel-1 GLCM textures contained most of the information needed for accurate classification. In general, the usefulness of SAR textures has also been demonstrated by an array of studies that involved the application of SAR textures derived from sensors other than Sentinel-1 for LULC classification. SAR textures played an influential role in many Land cover classification studies (e.g. De Alban et al. 2018; Laurin et al. 2012; Zhu et al. 2012). In our study, SAR textures derived from the VH polarization band with window size 11x11 made a notable difference in all cases. When combined, these texture measures alone produced OA accuracy of 60.37 with a 0.52 kappa coefficient value and they played an influential role in all the datasets that involved their contribution (Table 3).

In this study a dataset from the optical domain (Sentinel-2), consisting of 9 spectral bands (B1, B2, B3, B4, B5, B6, B7, B8A, B11, and B12 (20 m spatial resolution) provided OA of 88.12% and kappa coefficient value was 0.85. The inclusion of Sentinel-2 derived five

spectral indices (NDVI48, NDVI48a, NDVI56, NDVI57, and NDVI68a) helped increase the OA accuracy to 89.58% with a Kappa coefficient of 0.87. A four-layered optical (S2) dataset (B2, B3, B4, and B8 with 10 m spatial resolution) resulted in OA and Kappa index of 86.34 and 0.83 respectively whereas inclusion of NDVI in this dataset (5 variables) improved both OA accuracy (87.40%) as well as Kappa index (0.84).

Integration of SAR and optical data (S1+S2) which refers to feature level Optical -Radar data fusion further improved the classification accuracy than yielded by SAR or optical dataset alone. A data stack (25 layers) generated through the integration of 16 layers of SAR data (VH, VV texture features derived with window size 11x11) and 2 polarization bands) combined with 9 layers of optical data (spectral bands) produced an OA of 91.87% and a kappa coefficient of 0.90. The inclusion of five spectral indices (stack of 30 variables) further enhanced the classification accuracy, and this S1 + S2 data combination produced the highest overall accuracy of 93.12% (KC=0.91). In the case of 10 m spatial resolution spectral bands, a features stack, generated by integrating 14 VH, VV derived textures (11x11), 2 polarizations, and 4 spectral bands with NDVI layer (21 variables), resulted in 88.57% OA accuracy with KC=0.86. In the case of 10 m spatial resolution optical data, it proved to be the best SAR/Optical combination. Similarly, many other combinations of SAR and Optical data were tested for LULC classification. For example, S2 spectral bands (20 m) and SAR-derived texture measures (VH_7x7 and VV_11x11) combined with two polarization bands (25 feature layers) provided 89% of OA accuracy with a kappa coefficient of 0.87. The addition of five spectral indices to this combination (30 variables) made no difference and gave the same results (OA=89%, KC=0.87). Using another stack of 20 layers (VH_7, VV_9 textures with two polarizations and four 10 m

spectral bands) an OA accuracy of 86.40% (KC= 0.83) was obtained and similarly in another type of such combination that was developed by stacking four 10 m spectral bands and VH, VV SAR polarization bands (6 layers) OA accuracy of 86.71 (KC= 0.84) was achieved (Table 3).

Integrated use of SAR and Optical data, particularly Sentinel-1 and Sentinel-2 images have been used successfully in several studies aimed at LULC classification, forest and vegetation mapping, crop types identification, and in various other fields. Borges et al. 2020 conducted land cover mapping in Tanzanian Savanah where nine land cover classes were mapped by using S1 and S2 data through the Random Forest classification approach. The study concluded that optical models performed better than their radar counterparts and that overall accuracy for all given scenarios was improved by the combination of multi-sensor (S1+S2) data. The study also revealed that Sentinel-1 data was not able to distinguish well between most of the land cover classes and a higher degree of confusion was observed between forest, woodland, and bushland. It identified "Grassland' reasonably but overestimated the shrubland. Dobrinić et al. (2020) used S1 and S2 satellite data for classification of five land cover types in France. The classification results show that using RF classier S1 data provided an accuracy of 70.41% (KC=0.61) whereas S2-based results were better (Accuracy=84.17% with 0.80 Kappa Coefficient) than S1. The highest classification accuracy of 85.47% (KC=0.81) was achieved with the integrated use of S1 and S2 multisource data. The significance of SAR textures was also evident in the case of SAR-Optical data integration (S1+S2) where the indicated GLCM textures enhanced the overall accuracy from 89.58% (observed in the case of the optical dataset) to 93.12% with a corresponding increase in Kappa coefficient from 0.87 to 0.91

respectively. Here, again the recorded producer's and user's accuracies for the shrubland cover class have enhanced from 77%, 86% to 82%, and 91% respectively with the inclusion of texture features (calculated via window size 11x11).

Most of the cases that investigated the potential of SAR and optical data for LULC classification separately as well as in combination concluded that SAR data alone resulted in the lowest accuracy compared to which optical data performed better whereas the combination of both SAR and Optical data further improved the classification results and produced the highest overall accuracy. The findings of this study are well aligned with several studies (Lopes et al., 2020; Mercier et al., 2019; Poortinga et al., 2019; Tavares et al., 2019) that used Sentinel-1 and Sentinel-2 data for Random Forest based classification of LULC. These studies investigated the ability of Sentinel-1 and Sentinel-2 datasets for classification independently as well as in integration and ascertained that Sentinel-1 yielded the lowest accuracy. Sentinel-2 fetched better results relative to Sentinel-1 while the best overall accuracy was realized when S1 and S2 data were used in combined mode.

Conclusion

This study attempted to investigate the role of integrated use of freely and conveniently available SAR (Sentinel-1) and Optical (Sentinel-2) in an area with complex mountainous topography and different land cover classes. Three different scenarios were analyzed for the classification of land cover in the selected area of interest. An efficient machine learning classifier known as Random Forest was employed for classification and the achieved results were used to assess the accuracy of classification. The study reflects that feature-level Optical-SAR data fusion proved successful in improving OA classification

accuracy. The highest overall accuracy of 93.12% was observed when features derived from both SAR and Optical images were used in the integration. As signified in many studies, GLCM textures extracted from SAR polarization bands played an important role in this case in improving OA classification accuracy. Though observed increase in OA accuracy is only 3.5% yet it may prove very beneficial when LULC mapping is carried out at the level of State's extent. This finding may help and encourage resource managers and planners to conduct wall-wall LULC mapping across the State while utilizing free-of-charge and continuously available S1 and S2 data and sophisticated open-source software to prepare reports needed as a part of MRV reporting requirement under REDD+ that is an incentive-based mechanism aimed at mitigation of climate change impacts at the global level.

References

Abdel-Rahman, E. M., Mutanga, O., Adam, E., and Ismail, R. (2014). Detecting Sirex noctilio grey-attacked and lightning-struck pine trees using airborne hyperspectral data, random forest and support vector machines classifiers. ISPRS Journal of Photogrammetry and Remote Sensing 88: 48–59.

Abdikan, S., Sanli, F. B., Ustuner, M., and Calò, F. (2016). Land cover mapping using sentinel-1 SAR data. In International Archives of the Photogrammetry, Remote Sensing and Spatial Information Sciences - ISPRS Archives (Vol. 41). International Society for Photogrammetry and Remote Sensing.

Abdullah, A. Y. M., Masrur, A., Gani Adnan, M. S., Al Baky, M. A., Hassan, Q. K., and Dewan, A. (2019). Spatio-temporal patterns of land use/land cover change in the

heterogeneous coastal region of Bangladesh between 1990 and 2017. Remote Sensing 11(7).

Adam, E., Mutanga, O., Odindi, J., and Abdel-Rahman, E. M. (2014). Land-use/cover classification in a heterogeneous coastal landscape using RapidEye imagery: evaluating the performance of random forest and support vector machines classifiers. International Journal of Remote Sensing 35(10): 3440–3458.

Ali, M. Z., Qazi, W., and Aslam, N. (2018). A comparative study of ALOS-2 PALSAR and landsat-8 imagery for land cover classification using maximum likelihood classifier. Egyptian Journal of Remote Sensing and Space Science 21: S29–S35.

Amani, M., Mahdavi, S., Afshar, M., Brisco, B., Huang, W., Mohammad Javad Mirzadeh, S., White, L., Banks, S., Montgomery, J., and Hopkinson, C. (2019). Canadian Wetland Inventory using Google Earth Engine: The First Map and Preliminary Results. Remote Sensing 11(7): 842.

Awawdeh, M., Alkhateeb, E., and Al-Radaideh, N. (2023). The Use of Remote Sensing and GIS for Mapping Silica Sand Deposits in Jordan. Jordan Journal of Earth and Environmental Sciences 14(3): 232–240.

Bjerreskov, K. S., Nord-Larsen, T., and Fensholt, R. (2021). Forest type and tree species classification of nemoral forests with Sentinel-1 and 2 Time Series data.

Blickensdörfer, L., Schwieder, M., Pflugmacher, D., Nendel, C., Erasmi, S., and Hostert, P. (2022). Mapping of crop types and crop sequences with combined time series of Sentinel-1, Sentinel-2 and Landsat 8 data for Germany. Remote Sensing of Environment 269.

Borges, J., Higginbottom, T. P., Symeonakis, E., and Jones, M. (2020). Sentinel-1 and sentinel-2 data for savannah land cover mapping: Optimising the combination of sensors and seasons. Remote Sensing 12(23): 1–21.

Breiman, L. (2001). Random forests. (Robert E. Schapire, Ed.)Machine Learning. The Netherlands: Kluwer Academic Publishers.

Cai, Y., Lin, H., and Zhang, M. (2019). Mapping paddy rice by the object-based random forest method using time series Sentinel-1/Sentinel-2 data. Advances in Space Research 64(11): 2233–2244.

Cánovas-García, F., Alonso-Sarría, F., Gomariz-Castillo, F., and Oñate-Valdivieso, F. (2017). Modification of the random forest algorithm to avoid statistical dependence problems when classifying remote sensing imagery. Computers & Geosciences 103: 1–11.

Carrasco, L., O'Neil, A. W., Daniel Morton, R., and Rowland, C. S. (2019). Evaluating combinations of temporally aggregated Sentinel-1, Sentinel-2 and Landsat 8 for land cover mapping with Google Earth Engine. Remote Sensing 11(3).

Chowdhury, M. S. (2024). Comparison of accuracy and reliability of random forest, support vector machine, artificial neural network and maximum likelihood method in land use/cover classification of urban setting. Environmental Challenges 14(October 2023): 100800.

Clark, M. L. (2017). Comparison of simulated hyperspectral HyspIRI and multispectral Landsat 8 and Sentinel-2 imagery for multi-seasonal, regional land-cover mapping. Remote Sensing of Environment 200: 311–325.

Clerici, N., Valbuena Calderón, C. A., and Posada, J. M. (2017). Fusion of sentinel-1a and sentinel-2A data for land cover mapping: A case study in the lower Magdalena region, Colombia. Journal of Maps 13(2): 718–726.

Colson, D., Petropoulos, G. P., and Ferentinos, K. P. (2018). Exploring the Potential of Sentinels-1 & 2 of the Copernicus Mission in Support of Rapid and Cost-effective Wildfire Assessment. International Journal of Applied Earth Observation and Geoinformation 73: 262–276.

De Alban, J. D. T., Connette, G. M., Oswald, P., and Webb, E. L. (2018). Combined Landsat and L-band SAR data improves land cover classification and change detection in dynamic tropical landscapes. Remote Sensing 10(2).

Dobrinić, D., Medak, D., and Gašparović, M. (2020). Integration of multitemporal sentinel-1 and sentinel-2 imagery for land-cover classification using machine learning methods. In International Archives of the Photogrammetry, Remote Sensing and Spatial Information Sciences - ISPRS Archives (Vol. 43). International Society for Photogrammetry and Remote Sensing.

Gislason, P. O., Benediktsson, J. A., and Sveinsson, J. R. (2006). Random forests for land cover classification. Pattern Recognition Letters 27(4): 294–300.

Gómez, C., White, J. C., and Wulder, M. A. (2016, June 1). Optical remotely sensed time series data for land cover classification: A review. ISPRS Journal of Photogrammetry and Remote Sensing. Elsevier B.V.

Guo, L., Chehata, N., Mallet, C., and Boukir, S. (2011). Relevance of airborne lidar and multispectral image data for urban scene classification using Random Forests. ISPRS

Journal of Photogrammetry and Remote Sensing 66(1): 56–66.

Haas, J., and Ban, Y. (2018). Urban Land Cover and Ecosystem Service Changes based on Sentinel-2A MSI and Landsat TM Data. IEEE Journal of Selected Topics in Applied Earth Observations and Remote Sensing 11(2): 485–497.

Haralick, R. M., Shanmugam, K., and Dinstein, I. (1973). Textural Features for Image Classification. IEEE Transactions on Systems, Man, and Cybernetics SMC-3(6): 610–621.

Hdoush, A. A. azeez, Makhamreh, Z., Al-Weshah, R., and Qutishat, D. (2022). Land Suitability Evaluation Esing FAO Approach and Spatial Analysis for Mujib Basin – Jordan. Jordan Journal of Earth and Environmental Sciences 13(3): 158–167.

Heckel, K., Urban, M., Schratz, P., Mahecha, M. D., and Schmullius, C. (2020). Predicting forest cover in distinct ecosystems: The potential of multi-source Sentinel-1 and -2 data fusion. Remote Sensing 12(2).

Hu, B., Xu, Y., Huang, X., Cheng, Q., Ding, Q., Bai, L., and Li, Y. (2021). Improving urban land cover classification with combined use of sentinel-2 and sentinel-1 imagery. ISPRS International Journal of Geo-Information 10(8).

Hussain, S., Mubeen, M., Ahmad, A., Akram, W., Hammad, H. M., Ali, M., Masood, N., Amin, A., Farid, H. U., Sultana, S. R., Fahad, S., Wang, D., and Nasim, W. (2020). Using GIS tools to detect the land use/land cover changes during forty years in Lodhran District of Pakistan. Environmental Science and Pollution Research 27(32): 39676–39692.

Immitzer, M., Vuolo, F., and Atzberger, C. (2016). First experience with Sentinel-2 data for crop and tree species classifications in central Europe. Remote Sensing 8(3).

Inglada, J., Vincent, A., Arias, M., and Marais-Sicre, C. (2016). Improved early crop type identification by joint use of high temporal resolution sar and optical image time series. Remote Sensing 8(5).

Joshi, N., Baumann, M., Ehammer, A., Fensholt, R., Grogan, K., Hostert, P., Jepsen, M. R., Kuemmerle, T., Meyfroidt, P., Mitchard, E. T. A., Reiche, J., Ryan, C. M., and Waske, B. (2016). A review of the application of optical and radar remote sensing data fusion to land use mapping and monitoring. *Remote Sensing*. MDPI AG.

Kavitha, A. V., Srikrishna, A., and Satyanarayana, C. (2021). A Review on Detection of Land Use and Land Cover from an Optical Remote Sensing Image. IOP Conference Series: Materials Science and Engineering 1074(1): 012002.

Kelley, L. C., Pitcher, L., and Bacon, C. (2018). Using Google Earth Engine to Map Complex Shade-Grown Coffee Landscapes in Northern Nicaragua. Remote Sensing 10(6): 952.

Kussul, N., Lavreniuk, M., Skakun, S., and Shelestov, A. (2017). Deep Learning Classification of Land Cover and Crop Types Using Remote Sensing Data. IEEE Geoscience and Remote Sensing Letters 14(5): 778–782.

Lambin, E. F., Rounsevell, M. D. A., and Geist, H. J. (2000). Are agricultural land-use models able to predict changes in land-use intensity? Agriculture, Ecosystems and Environment 82(1–3): 321–331.

Laurin, G. V., Laurin, G. V., Balling, J., Corona, P., Mattioli, W., Papale, D., and Puletti, N. (2022). Above-ground biomass prediction by Sentinel-1 multitemporal data in central Italy with integration of ALOS2 and Sentinel-2 data. 12(1).

Laurin, G. V., Liesenberg, V., Chen, Q., Guerriero, L., Del Frate, F., Bartolini, A., Coomes, D., Wilebore, B., Lindsell, J., and Valentini, R. (2012). Optical and SAR sensor synergies for forest and land cover mapping in a tropical site in West Africa. International Journal of Applied Earth Observation and Geoinformation 21(1): 7–16.

Liu, Y., Gong, W., Hu, X., and Gong, J. (2018). Forest type identification with random forest using Sentinel-1A, Sentinel-2A, multi-temporal Landsat-8 and DEM data. Remote Sensing 10(6).

Lopes, M., Frison, P. L., Crowson, M., Warren-Thomas, E., Hariyadi, B., Kartika, W. D., Agus, F., Hamer, K. C., Stringer, L., Hill, J. K., and Pettorelli, N. (2020, April 1). Improving the accuracy of land cover classification in cloud persistent areas using optical and radar satellite image time series. *Methods in Ecology and Evolution*. British Ecological Society.

Mahdianpari, M., Salehi, B., Mohammadimanesh, F., and Motagh, M. (2017). Random forest wetland classification using ALOS-2 L-band, RADARSAT-2 C-band, and TerraSAR-X imagery. ISPRS Journal of Photogrammetry and Remote Sensing 130: 13–31.

Majeed, M., Tariq, A., Anwar, M. M., Khan, A. M., Arshad, F., Mumtaz, F., Farhan, M., Zhang, L., Zafar, A., Aziz, M., Abbasi, S., Rahman, G., Hussain, S., Waheed, M., Fatima, K., and Shaukat, S. (2021). Monitoring of land use–Land cover change and

potential causal factors of climate change in Jhelum district, Punjab, Pakistan, through GIS and multi-temporal satellite data. Land 10(10).

Maxwell, A. E., Strager, M. P., Warner, T. A., Ramezan, C. A., Morgan, A. N., and Pauley, C. E. (2019). Large-Area, High Spatial Resolution Land Cover Mapping Using Random Forests, GEOBIA, and NAIP Orthophotography: Findings and Recommendations. Remote Sensing 11(12): 1409.

Maxwell, A. E., Warner, T. A., and Fang, F. (2018). Implementation of machine-learning classification in remote sensing: an applied review. International Journal of Remote Sensing 39(9): 2784–2817.

Mendes, F. de S., Baron, D., Gerold, G., Liesenberg, V., and Erasmi, S. (2019). Optical and SAR remote sensing synergism for mapping vegetation types in the endangered Cerrado/Amazon ecotone of Nova Mutum-Mato Grosso. Remote Sensing 11(10).

Mercier, A., Betbeder, J., Rumiano, F., Baudry, J., Gond, V., Blanc, L., Bourgoin, C., Cornu, G., Ciudad, C., Marchamalo, M., Poccard-Chapuis, R., and Hubert-Moy, L. (2019). Evaluation of Sentinel-1 and 2 Time Series for Land Cover Classification of Forest–Agriculture Mosaics in Temperate and Tropical Landscapes. Remote Sensing 11(8): 979.

Millard, K., and Richardson, M. (2015). On the Importance of Training Data Sample Selection in Random Forest Image Classification: A Case Study in Peatland Ecosystem Mapping. Remote Sensing 7(7): 8489–8515.

Mongus, D., and Žalik, B. (2018). Segmentation schema for enhancing land cover identification: A case study using Sentinel 2 data. International Journal of Applied Earth

Observation and Geoinformation 66: 56–68.

Nuthammachot, N., and Stratoulias, D. (2019). Fusion of Sentinel-1a and Landsat-8 images for improving land use/land cover classification in Songkla Province, Thailand. Applied Ecology and Environmental Research 17(2): 3123–3135.

Orlíková, L., and Horák, J. (2019). Land cover classification using sentinel-1 SAR data. In ICMT 2019 - 7th International Conference on Military Technologies, Proceedings. Institute of Electrical and Electronics Engineers Inc.

Orynbaikyzy, A., Gessner, U., Mack, B., and Conrad, C. (2020). Crop type classification using fusion of sentinel-1 and sentinel-2 data: Assessing the impact of feature selection, optical data availability, and parcel sizes on the accuracies. Remote Sensing 12(17).

PNDD (2015). AZAD JAMMU & KASHMIR AT A GLANCE. Azad Jammu & Kashmir , Planning & Development Department, Bureau of Statistics .

Poortinga, A., Tenneson, K., Shapiro, A., Nquyen, Q., Aung, K. S., Chishtie, F., and Saah, D. (2019). Mapping plantations in Myanmar by fusing Landsat-8, Sentinel-2 and Sentinel-1 data along with systematic error quantification. Remote Sensing 11(7): 1–19.

Praticò, S., Solano, F., Di Fazio, S., and Modica, G. (2021). Machine Learning Classification of Mediterranean Forest Habitats in Google Earth Engine Based on Seasonal Sentinel-2 Time-Series and Input Image Composition Optimisation. Remote Sensing 13(4): 586.

Rodriguez-Galiano, V. F., Ghimire, B., Rogan, J., Chica-Olmo, M., and Rigol-Sanchez, J. P. (2012). An assessment of the effectiveness of a random forest classifier for land-cover classification. ISPRS Journal of Photogrammetry and Remote Sensing 67(1): 93–104.

Rodriguez-Galiano, Victor F., and Chica-Rivas, M. (2014). Evaluation of different machine learning methods for land cover mapping of a Mediterranean area using multi-seasonal Landsat images and Digital Terrain Models. International Journal of Digital Earth 7(6): 492–509.

Sandberg, M. (2016). Land cover mapping with multi-temporal SAR and optical satellite data. Aalto University.

Shrestha, B., Stephen, H., and Ahmad, S. (2021). Impervious surfaces mapping at city scale by fusion of radar and optical data through a random forest classifier. Remote Sensing 13(15).

Sukawattanavijit, C., Chen, J., and Zhang, H. (2017). GA-SVM Algorithm for Improving Land-Cover Classification Using SAR and Optical Remote Sensing Data. IEEE Geoscience and Remote Sensing Letters 14(3): 284–288.

Sylla, D., Mouissa, H., M-Cakadje-Konan, L., and Hauhouot, C. (2021). An object oriented classification approach for mapping land cover from Landsat and Sentinel image data in the north of Ivory Coast. Jordan Journal of Earth and Environmental Sciences 12(4): 337–343.

Tavares, P. A., Beltrão, N. E. S., Guimarães, U. S., and Teodoro, A. C. (2019). Integration of sentinel-1 and sentinel-2 for classification and LULC mapping in the

urban area of Belém, eastern Brazilian Amazon. Sensors (Switzerland) 19(5).

Teluguntla, P., Thenkabail, P. S., Oliphant, A., Xiong, J., Gumma, M. K., Congalton, R. G., Yadav, K., and Huete, A. (2018). A 30-m landsat-derived cropland extent product of Australia and China using random forest machine learning algorithm on Google Earth Engine cloud computing platform. ISPRS Journal of Photogrammetry and Remote Sensing 144: 325–340.

Tufail, R., Ahmad, A., Javed, M. A., and Ahmad, S. R. (2022). A machine learning approach for accurate crop type mapping using combined SAR and optical time series data. Advances in Space Research 69(1): 331–346.

Van Beijma, S., Comber, A., and Lamb, A. (2014). Random forest classification of salt marsh vegetation habitats using quad-polarimetric airborne SAR, elevation and optical RS data. Remote Sensing of Environment 149: 118–129.

Van Tricht, K., Gobin, A., Gilliams, S., and Piccard, I. (2018). Synergistic use of radar sentinel-1 and optical sentinel-2 imagery for crop mapping: A case study for Belgium. Remote Sensing 10(10).

Xia, J., Falco, N., Benediktsson, J. A., Du, P., and Chanussot, J. (2017). Hyperspectral Image Classification With Rotation Random Forest Via KPCA. IEEE Journal of Selected Topics in Applied Earth Observations and Remote Sensing 10(4): 1601–1609.

Zahid Khalil, R., and Saad-ul-Haque (2018). InSAR Coherence-based land cover classification of Okara, Pakistan. Egyptian Journal of Remote Sensing and Space Science 21: S23–S28.

Zakeri, H., Yamazaki, F., and Liu, W. (2017). Texture analysis and land cover classification of tehran using polarimetric synthetic aperture radar imagery. Applied Sciences (Switzerland) 7(5).

Zhang, H., Lin, H., and Li, Y. (2015). Impacts of feature normalization on optical and SAR data fusion for land use/land cover classification. IEEE Geoscience and Remote Sensing Letters 12(5): 1061–1065.

Zhang, H., Wang, T., Liu, M., Jia, M., Lin, H., Chu, L. M., and Devlin, A. T. (2018). Potential of combining optical and dual polarimetric SAR data for improving mangrove species discrimination Using Rotation Forest. Remote Sensing 10(3).

Zhang, R., Tang, X., You, S., Duan, K., Xiang, H., and Luo, H. (2020). A novel feature-level fusion framework using optical and SAR remote sensing images for land use/land cover (LULC) classification in cloudy mountainous area. Applied Sciences (Switzerland) 10(8).

Zhou, T., Zhao, M., Sun, C., and Pan, J. (2018). Exploring the impact of seasonality on urban land-cover mapping using multi-Season Sentinel-1A and GF-1 WFV images in a subtropical monsoon-climate region. ISPRS International Journal of Geo-Information 7(1).

Zhu, Z., Woodcock, C. E., Rogan, J., and Kellndorfer, J. (2012). Assessment of spectral, polarimetric, temporal, and spatial dimensions for urban and peri-urban land cover classification using Landsat and SAR data. Remote Sensing of Environment 117: 72–82.